Applied Surface Science 631 (2023) 157513

Contents lists available at ScienceDirect

Applied Surface Science

journal homepage: www.elsevier.com/locate/apsusc

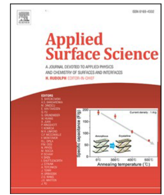

Full Length Article

Atomic resolution interface structure and vertical current injection in highly uniform MoS_2 heterojunctions with bulk GaN

F. Giannazzo [a,*], S.E. Panasci [a], E. Schilirò [a], G. Greco [a], F. Roccaforte [a], G. Sfuncia [a], G. Nicotra [a], M. Cannas [b], S. Agnello [b,a,c], E. Frayssinet [d], Y. Cordier [d], A. Michon [d], A. Koos [e], B. Pécz [e]

[a] Consiglio Nazionale delle Ricerche – Istituto per la Microelettronica e Microsistemi (CNR-IMM), Z.I. VIII Strada 5, 95121 Catania, Italy
[b] Department of Physics and Chemistry Emilio Segré, University of Palermo, Via Archirafi 36, 90143 Palermo, Italy
[c] AtenCenter, University of Palermo, Viale delle Scienze Ed.18, 90128 Palermo, Italy
[d] Université Côte d'Azur, CNRS, CRHEA, 06560 Valbonne, France
[e] Centre for Energy Research, Institute of Technical Physics and Materials Science, Budapest, Hungary

ARTICLE INFO

Keywords:
MoS_2
Bulk GaN
Heterojunctions
Aberration corrected TEM
Conductive AFM

ABSTRACT

The integration of two-dimensional MoS_2 with GaN recently attracted significant interest for future electronic/optoelectronic applications. However, the reported studies have been mainly carried out using heteroepitaxial GaN templates on sapphire substrates, whereas the growth of MoS_2 on low-dislocation-density bulk GaN can be strategic for the realization of "truly" vertical devices. In this paper, we report the growth of ultrathin MoS_2 films, mostly composed by single-layers (1L), onto homoepitaxial n^--GaN on n^+ bulk substrates by sulfurization of a pre-deposited MoO_x film. Highly uniform and conformal coverage of the GaN surface was demonstrated by atomic force microscopy, while very low tensile strain (~0.05%) and a significant p^+-type doping (~4.5×10^{12} cm^{-2}) of 1L-MoS_2 was evaluated by Raman mapping. Atomic resolution structural and compositional analyses by aberration-corrected electron microscopy revealed a nearly-ideal van der Waals interface between MoS_2 and the Ga-terminated GaN crystal, where only the topmost Ga atoms are affected by oxidation. Furthermore, the relevant lattice parameters of the MoS_2/GaN heterojunction, such as the van der Waals gap, were measured with high precision. Finally, the vertical current injection across this 2D/3D heterojunction has been investigated by nanoscale current-voltage analyses performed by conductive atomic force microscopy, showing a rectifying behavior with an average turn-on voltage $V_{on} = 1.7$ V under forward bias, consistent with the expected band alignment at the interface between p^+ doped 1L-MoS_2 and n-GaN.

1. Introduction

In the last years, the integration of two dimensional (2D) transition metal dichalcogenides, such as the molybdenum disulfide (2H-MoS_2) [1], with wide-bandgap (WBG) semiconductors, including silicon carbide (4H-SiC) [2,3], gallium nitride (GaN) [4,5] and AlGaN alloys [6], has been the object of increasing research interest. In fact, the combination of the unique physical properties of ultrathin MoS_2 films, such as the tunable energy bandgap [7,8] and the relatively high in-plane carrier mobility [9], with the robust electronic properties of SiC and GaN (wide-bandgap, high breakdown field and electron saturation velocity) [10,11] paves the way to novel device concepts, including heterojunction diodes based on the vertical current injection at the 2D/3D semiconductors interfaces [12,13], and optoelectronic devices (e.g., dual wavelength photodetectors) exploiting the optical response of these materials in the visible and UV spectral ranges [14,15]. Due to this wide application potential, several approaches have been explored to fabricate MoS_2 heterojunctions with SiC and GaN, including exfoliation of MoS_2 flakes from bulk crystals [6,14,15], transfer of MoS_2 thin films grown on foreign substrates [12,13], and the direct MoS_2 growth on SiC and GaN substrates by scalable approaches like chemical vapor deposition (CVD) [16,17] and pulsed laser deposition (PLD) [18,19,20]. In particular, the epitaxial growth of MoS_2 on these hexagonal symmetry WBG substrates is favored by the very low lattice parameter mismatch in the basal planes, ~2.9% in the case of SiC(0001) [20] and <1% for GaN (0001) [16].

Recent reports on heterojunction diodes formed by monolayer (1L) or few layers MoS_2 grown on 4H-SiC bulk crystals already showed very

* Corresponding author.
E-mail address: filippo.giannazzo@imm.cnr.it (F. Giannazzo).

https://doi.org/10.1016/j.apsusc.2023.157513
Received 5 February 2023; Received in revised form 7 April 2023; Accepted 10 May 2023
Available online 15 May 2023
0169-4332/© 2023 The Authors. Published by Elsevier B.V. This is an open access article under the CC BY license (http://creativecommons.org/licenses/by/4.0/).

promising performances for vertical devices applications [20,21]. On the other hand, although MoS_2 integration with GaN has been more widely investigated, the majority of studies has been performed using heteroepitaxial GaN films grown on insulating sapphire substrates [16,17]. Despite the high density of threading dislocations ($\sim 10^8$–10^9 cm^{-2}) [22], originating from the lattice and thermal expansion coefficient mismatch with the substrate, low-cost heteroepitaxial GaN on sapphire is widely employed in optoelectronics, whereas GaN grown on Si and on semi-insulating SiC are employed in medium-voltage (650–900 V) power transistors and RF transistors, respectively. On the other hand, low-dislocation-density ($<10^5$ cm^{-2}) n-GaN homoepitaxial layers on n^+ bulk GaN [22] are necessary for the implementation of vertical transistors and diodes, allowing to fully exploit the potential of GaN at higher voltage/current rating [23]. Although free-standing GaN still remain high-cost substrates, large improvement in the bulk growth methods have been made during last decade [24], and high quality bulk GaN wafers up to 100 mm diameter are now available.

As a matter of fact, the high dislocation density in heteroepitaxial GaN on sapphire is expected to significantly affect the rectification properties of the MoS_2/GaN interface. In this respect, the integration of ultra-thin MoS_2 films on low defectivity homoepitaxial GaN layers can be extremely beneficial, both to explore the "intrinsic" rectification properties of the MoS_2/GaN interface and for the future development of 2D/3D vertical devices for high power and high frequency applications. However, only few studies have been reported so far about MoS_2 growth on bulk GaN, and they have been limited to the case of multilayer MoS_2 on a n^+ doped (10^{18} cm^{-3}) GaN substrate [25].

In this paper we report on the highly uniform growth of ultrathin MoS_2, mostly formed by monolayer (1L) or bilayers (2L), on top of homoepitaxial GaN by a two-steps chemical vapor deposition (CVD) approach, consisting in the sulfurization of a pre-deposited ultrathin MoO_x film. As compared to the commonly employed single-step CVD with S and MoO_3 vapours, typically resulting in the nucleation and growth of isolated triangular domains of MoS_2, this method allows to obtain continuous MoS_2 films on large area with good thickness uniformity by controlling the initial MoO_x thickness [21,26]. In particular, the surface morphology of as-grown MoS_2 films was demonstrated to be very conformal to the atomic steps of n-GaN homoepitaxy. Atomic resolution structural and compositional analyses, carried out by aberration-corrected transmission electron microscopy combined with electron energy loss spectroscopy (EELS), revealed a nearly-ideal van der Waals (vdW) interface between MoS_2 and the Ga-terminated GaN crystal, where only the topmost Ga atoms are affected by oxidation. Furthermore, these analyses provided a precise evaluation of the relevant lattice parameters of the heterojunction, such as a vdW gap ranging from 4.71 to 5.06 Å. These atomic scale investigations were complemented by micro-scale Raman mapping with high statistics, which revealed a very low tensile strain at MoS_2/GaN interface, consistently with the lattice matching of the two crystals, and a significant p^+-type doping of MoS_2, ascribed to MoO_x residues. Finally, the vertical current injection across this 2D/3D heterojunction has been investigated by local current-voltage analyses performed by conductive atomic force microscopy (C-AFM), which showed a rectifying behavior with an average turn-on voltage $V_{on} = 1.7$ V under forward bias, consistent with the expected band alignment at p^+ MoS_2/n-GaN interface.

2. Experimental details

The starting material for our MoS_2 growth experiments was a $\sim$300 μm thick GaN substrate, Ga polarity (0001) oriented and n^+-doped (N_D-N_A = 1–5 × 10^{18} cm^{-3}), covered by a $\sim$3 μm thick n^- GaN homoepitaxial layer (N_D-$N_A \approx 1 \times 10^{16}$ cm^{-3}). An heteroepitaxial GaN template, grown by metal organic chemical vapor deposition (MOCVD) on sapphire, was also employed for benchmarking purposes. A MoO_x film (with $\sim$1.5 nm thickness, evaluated by AFM-step height measurements) was deposited on the GaN surface by DC magnetron sputtering from a Mo target using a Quorum Q300-TD equipment, followed by natural oxidation in air. Afterwards, the sulfurization process was carried out in a two-heating horizontal furnace, hosting a crucible with S powders in the low temperature zone (T_1 = 150 °C) and the MoO_x/GaN sample in the high temperature zone (T_2 = 700 °C). Argon was used as the carrier gas to transport the S vapour to the sample's surface and the process duration was 1 h. The same sulfurization conditions have been recently employed for MoO_x films with similar thickness on 4H-SiC, resulting in the formation of a highly uniform 1L-2L MoS_2 film [21].

The composition of the as-deposited MoO_x films before sulfurization was preliminary evaluated by XPS analyses, carried out using an XSAM 800 instrument by Kratos Analytical, with a non-monochromatic Mg Kα X-ray source (energy = 1253.6 eV). Mo 3d core level spectra are reported in Fig.S1 of the Supplementary Information, from which a stoichiometry MoO_x, with x = 2.8, was deduced. The coverage uniformity of the MoS_2 films on GaN has been first investigated by tapping mode AFM with a DI-3100 system by Bruker using ultra-sharp Si tips ($\sim$5 nm curvature radius). Furthermore, the distribution of the number of MoS_2 layers, strain and doping were evaluated by micro-Raman spectroscopy and mapping with a 532 nm laser wavelength, carried out using a WiTec Alpha and a Horiba equipment. The structural and chemical properties of the MoS_2 films on GaN have been investigated at atomic resolution by transmission electron microscopy on cross-sectioned lamellas, prepared by focused-ion-beam (FIB). First, high-resolution transmission electron microscopy (HRTEM), scanning transmission electron microscopy (STEM) in high-angle-annular-dark-field (HAADF) mode, and energy dispersion spectroscopy (EDS) analyses were acquired using an image corrected ThermoFisher THEMIS 200 microscope with 200 keV electron beam. Furthermore, atomic resolution analyses of the MoS_2/GaN interface by STEM in the HAADF and annular bright field (ABF) modes, and chemical mapping by electron energy loss spectroscopy (EELS) have been performed using a probe corrected JEOL ARM 200F microscope at primary electron beam energy of 200 keV. Finally, the vertical current injection in MoS_2 heterojunctions with bulk GaN was investigated by nanoscale resolution current-voltage (I-V) analyses in the front-to-back configuration performed by conductive AFM (C-AFM) with a DI-3100 system by Bruker, using Pt-coated conductive tips.

3. Results and discussion

Fig. 1(a) shows a representative AFM morphological image of the as-grown MoS_2 on the n^- homoepitaxial GaN sample, confirming the formation of a homogenous film, highly conformal to the atomic steps of the GaN surface, as evident from the higher resolution image in Fig. 1 (b). The scanned area in Fig. 1(a) includes some scratches, intentionally performed in the film in order to evaluate its thickness by step height measurements. Fig. 1(c) shows a height line profile, extracted along the red-line in Fig. 1(a), from which $\sim$0.7 nm film thickness is deduced in the considered region, which is in the range of typical thickness values for 1L-MoS_2 measured by AFM. This value is also in good agreement with the distance between the topmost S plane of MoS_2 and the topmost Ga plane of the (0 0 0 1) oriented GaN, evaluated by atomic resolution STEM in this paper.

In the following, the results of Raman mapping will be reported, to evaluate the distribution of the number of MoS_2 layers, the doping and strain on large areas and with high statistics. A typical Raman spectrum of the MoS_2 heterostructure with bulk GaN is shown in Fig. 2(a), where the vibrational peaks of MoS_2 (E_{2g} and A_{1g}) and GaN (E_2 high energy and A_1(LO)) are indicated by red and blue boxes, respectively. Furthermore, Fig. 2(b) reports a detail of the MoS_2 spectrum, showing the out-of-plane (A_{1g}) and the in-plane (E_{2g}) modes located at 406.0 ± 0.6 cm^{-1} and 384.6 ± 0.6 cm^{-1}, respectively. In addition to the two main E_{2g} and A_{1g} modes, the presence of additional spectral contributions, i.e. the LO(M) mode at $\sim$380.5 cm^{-1} and ZO(M) mode at $\sim$414.5 cm^{-1}, has been revealed by the deconvolution analysis in Fig. 2(b). These contributions, typically associated to MoS_2 lattice defects [27], can be related to the

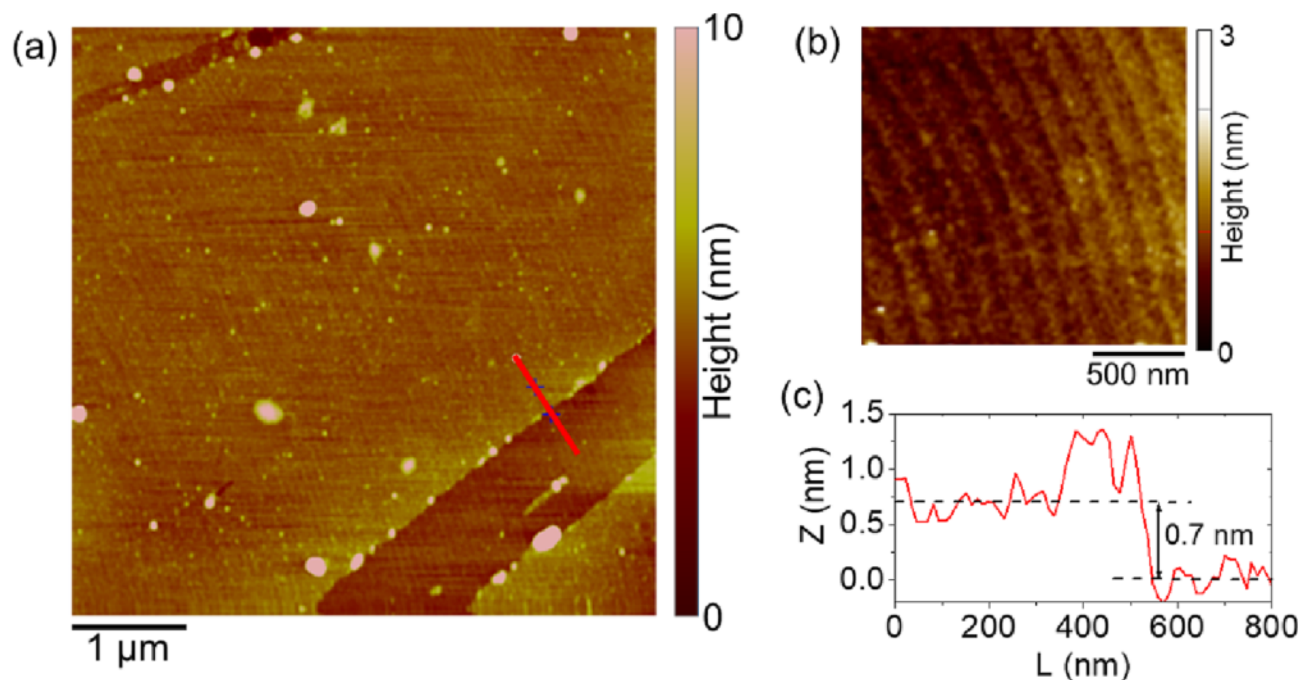

Fig. 1. (a) AFM image showing the as-grown MoS_2 on GaN morphology. The scanned area includes scratches intentionally performed in the MoS_2 film to evaluate its thickness (b) Higher resolution image showing conformal coverage on the GaN surface atomic steps. (c) Line profile extracted along the red line indicated in the panel (a). (For interpretation of the references to colour in this figure legend, the reader is referred to the web version of this article.)

grain boundaries of the polycrystalline MoS_2 layers produced by sulfurization of MoO_x films deposited by evaporation or sputtering. The typical size of MoS_2 crystalline domains in these layers, evaluated by plan-view TEM analyses, is in the range from few tens of nm to ~100 nm, depending on the substrate and on the sulfurization temperature [28,29,30,31,32]. Similarly, we estimated a domain size of 50–60 nm for our MoS_2 films transferred on a TEM grid.

The wavenumber difference $\Delta\omega = \omega_{A1g}$-$\omega_{E2g}$ between the A_{1g} and E_{2g} peaks is commonly used to estimate the number of MoS_2 layers [33,34]. Hence, to evaluate the MoS_2 thickness uniformity on the bulk GaN, we performed a statistical analysis over an array of 50 × 50 Raman spectra collected on a 10 μm × 10 μm sample area. The result of this analysis is represented by the $\Delta\omega$ histogram in Fig. 2(c). As indicated in the upper horizontal scale, the $\Delta\omega$ values in the range between ~19 and ~21.7 cm^{-1} correspond to 1L-MoS_2, the values between ~21.7 and ~23.1 cm^{-1} to 2L-MoS_2, the values between ~23.1 and ~24.2 cm^{-1} to 3L-MoS_2, and the values and >24.2 cm^{-1} to 4L-MoS_2 and thicker films. By integrating the counts in each $\Delta\omega$ range, a 1L-MoS_2 percentage of ~73%, 2L-MoS_2 percentage of ~24%, 3L-MoS_2 percentage of ~2%, and 4L-MoS_2 percentage of ~1% have been estimated.

In addition to the determination of the number of layers, the positions of the two main Raman peaks allow to evaluate the strain and doping of the ultra-thin MoS_2 membrane [35], resulting by the growth conditions and the interaction with the GaN substrate. Fig. 2(d) shows a correlative plot of the A_{1g} vs E_{2g} peak positions extracted from the array of Raman spectra. In particular, the (ω_{A1g}, ω_{E2g}) data points belonging to 1L-MoS_2 (i.e. those with $\Delta\omega < 21.7$ cm^{-1}) have been indicated by black dots, and the data points belonging to thicker (2L, 3L, 4L) MoS_2 regions have been indicated by blue dots. The red and black lines are the strain and doping lines, respectively, which represent the theoretical correlations between the vibrational frequencies of a purely strained and of a purely doped 1L-MoS_2 [36,37,38]. These two lines cross in a point (grey square) corresponding to the E_{2g} and A_{1g} wavenumbers for an ideally unstrained and undoped 1L-MoS_2 [37]. Here, the literature values ω_{E2g} = 385 cm^{-1} [37] and ω_{A1g} = 405 cm^{-1} [37] for a suspended 1L-MoS_2 membrane have been assumed as the best approximation for this ideal case. The experimental points are centered in the upper (blue) region of the plot, indicating a significant p-type doping of MoS_2. In particular, from the black data points an average hole density $p \approx 4.5 \times 10^{12}$ cm^{-2} was estimated for 1L-MoS_2. Furthermore, 1L-MoS_2 exhibits a very small tensile strain (average value ~0.05%), consistently with the small mismatch (<1%) between the in-plane lattice parameters of MoS_2 and GaN [2]. The origin of the p-type doping can be ascribed to the presence of MoO_x residues in the MoS_2 thin films produced by the sulfurization process. This aspect has been explained and demonstrated by XPS analysis in our previous work, in which we employed the same growth conditions for the MoS_2 on 4H-SiC [21].

It is worth mentioning that, for benchmarking purposes, similar micro-Raman mapping and statistical analyses have been carried out on MoS_2 films grown under identical conditions on the GaN-on-sapphire template. The results of this investigation (reported in Fig.S2 of the supporting information) indicated very similar distributions in the MoS_2 layers number, doping and strain, demonstrating the growth process reproducibility on homo- and hetero-epitaxial GaN samples.

After this statistical characterization of the as-grown MoS_2 film on micrometer scale areas, the structural and chemical properties of MoS_2 interface with homoepitaxial GaN were investigated at nanometric/atomic scale by transmission electron microscopy and spectroscopy. Fig. 3(a) shows a low magnification cross-sectional TEM image, confirming the presence of a continuous layered film, composed by 1L or 2L MoS_2, on the GaN surface. The amorphous carbon film with the nanocrystalline Pt on top served as protection for MoS_2 layers during FIB preparation. Noteworthy, TEM analyses at the same magnification, carried out on MoS_2 films grown on the GaN-on-sapphire templates (see Fig.S3 in the Supporting Information), showed the same MoS_2 film coverage, consistently with Raman results, while the main difference consisted in the presence of threading dislocations in the heteroepitaxial GaN crystal.

To get atomically resolved information on the MoS_2/GaN interface structure, STEM analyses have been simultaneously performed in the HAADF and the ABF imaging modes, as reported in Fig. 3(b) and (c), respectively. In the HAADF image, obtained by collecting electrons scattered at large angles, the bright contrast is associated to the columns of atoms (i.e., Mo, Ga) with high atomic number (Z), whereas the low Z

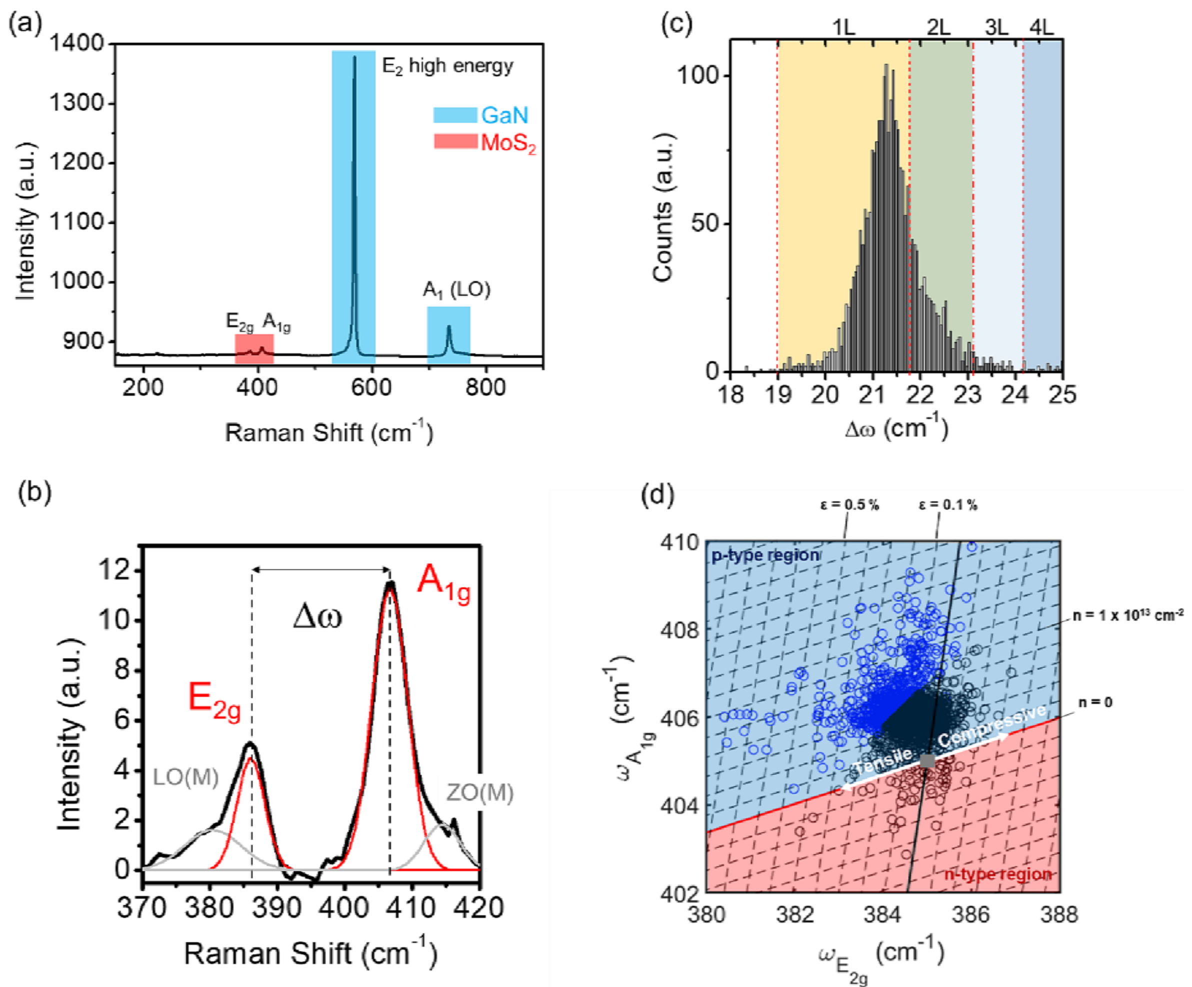

Fig. 2. (a) Raman spectrum of the 2D/3D heterojunction with the corresponding MoS_2 (red square) and GaN (blue squares) peaks. (b) Detail on the MoS_2 in-plane (E_{2g}) and out-of-plane (A_{1g}) peaks after the deconvolution analysis from which the presence of further peaks defined LO(M) and ZO(M) can be appreciated. (c) Distribution of the difference ($\Delta\omega = \omega_{A1g}$- ω_{E2g}) between the two MoS_2 Raman peaks obtained from an array of 2500 spectra collected over a 10 μm × 10 μm sample area. The number of MoS_2 layers corresponding to the different Δω ranges is indicated in the upper horizontal scale. (d) Correlative E_{2g} vs A_{1g} plot to extract information on the strain and doping of MoS_2. Black points correspond to 1L-MoS_2 regions, whereas the blue points correspond to thicker MoS_2 regions. (For interpretation of the references to colour in this figure legend, the reader is referred to the web version of this article.)

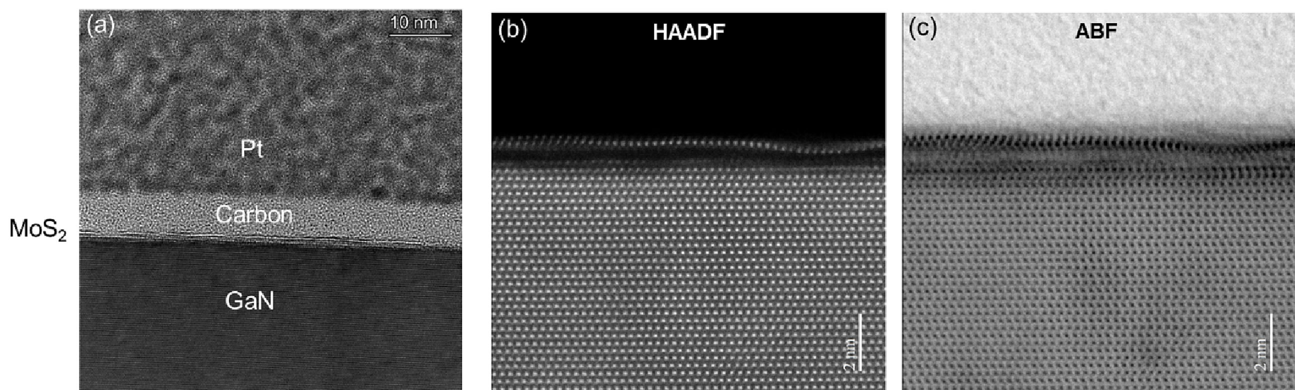

Fig. 3. (a) Low magnification TEM image of the MoS_2 film grown onto the n$^-$ GaN homoepitaxial layer on the bulk GaN substrate. Atomic resolution STEM images acquired in the HAADF mode (b) and ABF mode (c).

atoms (i.e., N and S) are difficult to be imaged. On the other hand, in the ABF imaging mode both atoms with high and lower Z can be simultaneously visualized as dark spots with higher and lower intensities, respectively. The combination of these two complementary imaging modes allowed a precise evaluation of the relevant lattice distances in the heterostructure, as shown later in this paper. Looking in detail to the near-interface GaN lattice, a first interesting feature that can be observed in the HAADF images is a reduced intensity of the topmost Ga

atomic plane with respect to the underlying GaN crystal. Previously reported STEM investigations of MoS_2 on GaN (grown by single-step CVD at 800 °C) also reported on the presence of a "modified" GaN surface region, formed by two GaN planes underneath MoS_2 [17]. Such modification was tentatively explained by the authors in terms of the GaN surface reconstruction or its partial oxidation during the MoS_2 growth, but these hypotheses were not conclusively supported by the reported electron microscopy analyses, due to the insufficient resolution and lack of chemical information [17].

Here, the compositional properties of the MoS_2/GaN heterostructure were investigated in detail by EELS and elemental mapping (as shown in Fig. 4) and by EDS (as reported in Fig.S4 of the Supporting Information). Fig. 4(a) displays an overview EELS spectrum, collected in the region shown in the HAADF spectrum image of Fig. 4(b). The spectral features associated to the main atomic species present in the heterostructure, i.e, the Ga-M and Ga-L edges, the N-K edge, the S-L edge and the Mo-M edge, are clearly detected. Furthermore, the presence of a weak intensity O-K peak was also observed. The chemical maps, showing the spatial distribution of the different atomic species in the spectrum image region, are reported in Fig. 4(c)-(h). Besides confirming MoS_2 formation, these analyses demonstrated that the near-surface GaN region is almost unaffected by the sulfurization of the pre-deposited MoO_x film at 700 °C, except for the incorporation of oxygen traces. The presence of a very small amount of oxygen also in the MoS_2 region can be deduced from the EELS map of Fig. 4(g), and it is confirmed by the EDS analyses in Fig.S3. It can be associated to some MoO_x residues still present after the sulfurization, as previously observed by XPS analyses on samples prepared under similar conditions [21]. Such small percentages of MoO_x can be relevant for the electronic properties of MoS_2, since they can produce a p-type doping of the layer, as revealed by Raman analyses (see Fig. 2 (d)).

To get further information on the atomic structure of near interface region, Fig. 5(a) and (c) show two atomic resolution STEM analyses, simultaneously collected in the HAADF (a) and ABF (c) imaging modes, respectively. The intensity line profiles, averaged on the individual atomic planes, are superimposed on the left and right sides of the two images. Accurate estimations of the lattice distances in the direction perpendicular to the interface were obtained by measuring the distances between the peaks in these line profiles.

Firstly, the peak in the HAADF line profile corresponding to the topmost Ga plane exhibits a significantly lower intensity as compared to the underlying Ga atomic planes. Furthermore, the separation between the 1st and the 2nd Ga planes (ranging from 2.89 to 3.27 Å) is significantly larger than the one between the 2nd and the 3rd Ga planes (~2.60 Å), which is the same for the underlying bulk GaN crystal. A distance $d_{Ga\text{-}Mo}$ between the topmost Ga plane of GaN and the plane of Mo atoms of the MoS_2 film ranging from 6.26 to 6.61 Å was also evaluated from the HAADF intensity line-profile in Fig. 5(a). Further insights on the S-Mo-S distances within 1L-MoS_2, and the S-Ga distance between the bottom S atoms of MoS_2 and the topmost Ga plane of the substrate have been deduced from the ABF image and intensity line profile in Fig. 5(c). Firstly, we observed slightly different distances ($d_{S\text{-}Mo} = 1.68$ Å and $d_{Mo\text{-}S} = 1.55$ Å) between the central Mo atoms and the upper and lower S planes of 1L-MoS_2. Furthermore, a vdW gap $d_{S\text{-}Ga}$ ranging from 4.71 to 5.06 Å between the lower S plane and the topmost Ga was evaluated from Fig. 5(c). Finally, the larger separation between the 1st and 2nd Ga atomic plane was explained by the substitution of oxygen to nitrogen atoms, i.e. by the formation of GaO_x, as schematically illustrated in Fig. 5(b). This view is also consistent with the results of chemical analysis reported in Fig. 4.

After assessing the strain, doping and interface structural properties of ultrathin MoS_2 on bulk GaN, the electrical properties of MoS_2 films and the vertical current injection across the MoS_2/GaN vdW heterojunction were investigated by nanoscale resolution current-voltage analysis based on C-AFM.

The current injection from the C-AFM tip to MoS_2 was preliminary evaluated, as discussed in Fig.S5 of the Supporting Information, showing a behavior consistent with p^+-doping of MoS_2. Afterwards, front-to-back current measurements from the nanometric Pt tip contact with MoS_2 surface to the macroscopic Ni/Au back-contact with n^+- bulk GaN, have been performed, according to the configuration illustrated in the insert of Fig. 6(a). A dc bias ramp is applied between these two contacts, while

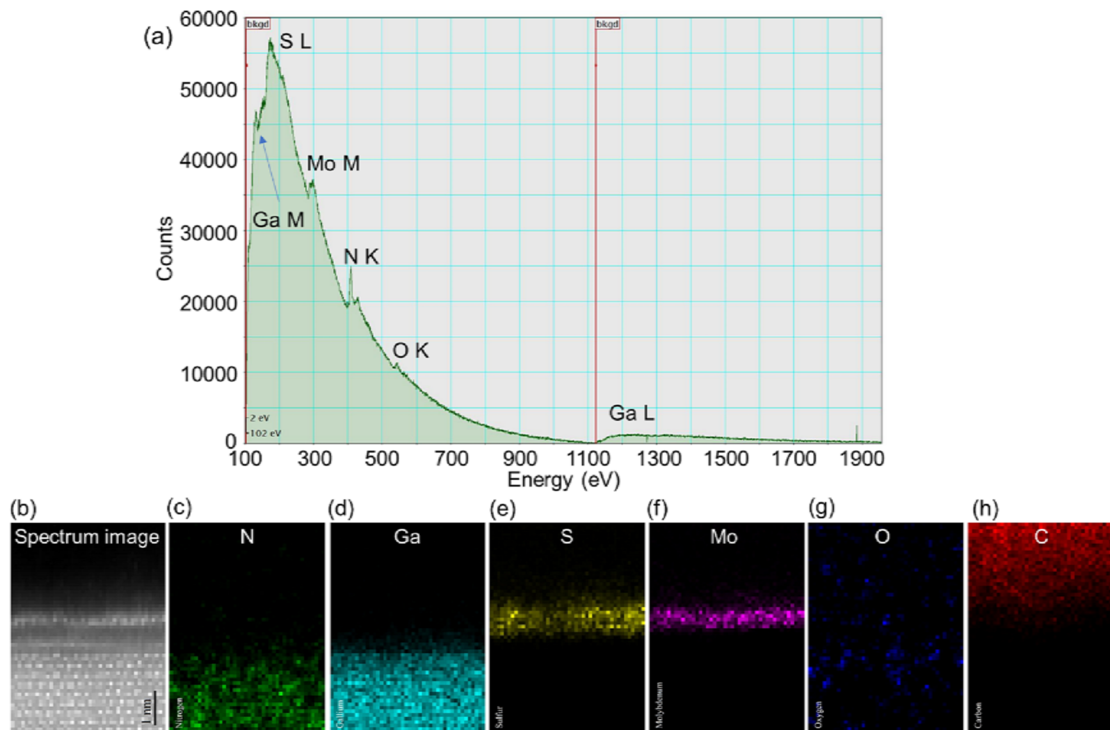

Fig. 4. (a) EELS spectrum of the MoS_2/GaN heterostructure, with the indication of edges of the detected atomic species. HAADF spectrum image of the analyzed region (b) and corresponding elemental maps of Nitrogen (c), Gallium (d), Sulfur (e), Molybdenum (f) Oxygen (g) and Carbon (h).

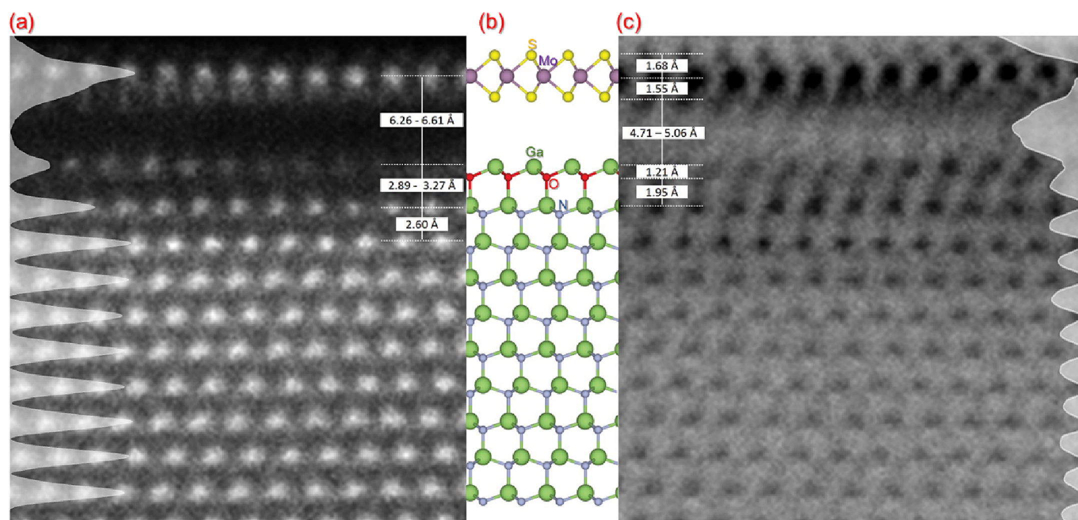

Fig. 5. Atomic resolution cross-sectional STEM of 1L-MoS_2/GaN heterostructure in HAADF (a) and ABF (c) imaging modes. The intensity line profiles, averaged on the individual atomic planes, are superimposed on the left and right sides of the two images. (c) Schematic representation of the atomic arrangement in the heterostructure. The Mo-Ga and Ga-Ga inter-plane distances were evaluated from the HAADF intensity profiles. The S-Mo-S distances within 1L-MoS_2, the S-Ga van der Waals gap, and the Ga-O distance in GaOx surface were evaluated from the ABF intensity profiles.

the flowing current is measured by a high sensitivity current amplifier connected to the tip. Fig. 6(a) shows a set of local I-V_{tip} curves measured on an array of 5 × 5 tip positions on 5 μm × 5 μm area. As can be seen, the I-V_{tip} curves, reported on a semi-log scale, showed a rectifying behavior, with a negligible current under reverse bias and an exponential rise of the current under forward bias above an onset voltage (V_{on}). The histogram in Fig. 6(b) represents the distribution of the V_{on} values extracted from the I-V_{tip} curves array at a fixed value of the threshold current $I_{th} = 1 \times 10^{-13}$ A (above the noise level), as indicated in Fig. 6(a). This distribution exhibits an average value of ~1.7 V, with a standard deviation of ±0.4 V. The very low reverse current and the relatively high onset voltage in the I-V_{tip} curves indicates a high energy barrier for current injection at MoS_2/GaN interface.

Fig. 6(c) schematically illustrates the energy band diagram of the heterojunction before the 1L-MoS_2/GaN contact formation. The type II band alignment is deduced from recent literature reports based on XPS/UPS analyses of the 1L-MoS_2/GaN system, where conduction band discontinuity ΔE_c values in the range from 0.07 to 0.6 eV have been evaluated [4,39]. The Fermi level position (E_F-$E_{C,GaN} \approx -0.11$ eV) in the n^- GaN epitaxy was estimated from the nominal doping level ($N_D \approx 1 \times 10^{16}$ cm^{-3}) according to the relation E_F-$E_{C,GaN} = kT/q \ln(N_D/N_C)$, being $N_C = 1.8 \times 10^{18}$ cm^{-3} the effective density of states in the conduction band at T = 300 K for GaN [40], k the Boltzmann constant and q the electron charge. On the other hand, the average hole density (p≈4.5 × 10^{12} cm^{-2}) in the p-type doped 1L-MoS_2, evaluated by Raman mapping in Fig. 2(d), corresponds to an average concentration of $N_h \approx 1.4 \times 10^{20}$ cm^{-3}, assuming that this charge is confined within an effective thickness of ~3.23 Å for 1L-MoS_2, as evaluated by the ABF TEM (see Fig. 5(c)). Such a value is larger than the effective density of states in the valence band $N_v \approx 1.2 \times 10^{19}$ cm^{-3} for 1L MoS_2, estimated by using a parabolic valence-band model and the corresponding analytical formula $N_V = 2(2\pi m_h kT/h^2)^{3/2}$, where h is the Planck constant, T = 300 K, and $m_h = 0.61 m_e$ is the holes effective mass for 1L-MoS_2. Hence, a degenerately p-type-doped 1L-MoS_2, with the Fermi level very close to the valence band edge (or inside the valence band) can be assumed, as schematically depicted in Fig. 6(c). Finally, the energy band diagram configuration of this p^+/n^- 2D/3D heterojunction after contact formation (under equilibrium conditions) is schematically illustrated in Fig. 6(d), where Φ_B indicates the energy barrier after the Fermi levels alignment. According to this band diagram, Φ_B can be estimated as $\Phi_B = E_{g,1L\text{-}MoS2}$-$|E_F$-$E_{C,GaN}|$, being $E_{g,1L\text{-}MoS2}$ the bandgap of 1L-MoS_2 (i.e., 1.8–1.9 eV) and $|E_F$-$E_{C,GaN}| \approx 0.11$ eV. This value is consistent with the average onset voltage ($V_{on} = 1.7$ V) previously extracted from the I-V_{tip} characterization, while the spread (±0.4 V) of the local V_{on} values (histogram in Fig. 6(d)) can be ascribed to local variations of MoS_2 p-type doping, resulting in local changes of the energy band alignment.

4. Conclusion

In conclusion, the growth of uniform MoS_2 films, mostly composed by single-layers, onto homoepitaxial n^--GaN on n^+ bulk substrates has been obtained by sulfurization at 700 °C of a pre-deposited MoO_x film. The grown MoS_2 layers are highly conformal to the GaN surface atomic steps. They exhibit very low tensile strain (~0.05%), consistently with the low in-plane lattice mismatch between MoS_2 and GaN, and a significant p^+- doping (average holes density p ≈ 4.5 × 10^{12} cm^{-2}), that was ascribed to residual MoO_x from the sulfurization process. A nearly-ideal vdW interface between MoS_2 and the Ga-terminated GaN crystal, where only the topmost Ga atoms are affected by oxidation, was demonstrated by atomic resolution STEM in the HAADF and ABF modes, combined with EELS. The relevant lattice parameters of the MoS_2/GaN heterojunction were measured with high precision. Finally, the vertical current injection across this 2D/3D heterojunction was investigated by nanoscale current-voltage analyses performed by conductive AFM, showing a rectifying behavior with an average turn-on voltage $V_{on} \approx 1.7$ V under forward bias, consistent with the expected band alignment at p^+-MoS_2/n-GaN interface.

The obtained results on the integration of highly uniform and ultrathin p^+ MoS_2 films with low-dislocation density n^- GaN homoepitaxial layers, and the demonstration of the rectifying electrical behavior of this 2D/2D heterostructure are important steps towards the development of vertical heterojunction diodes for high-power and high-frequency applications.

CRediT authorship contribution statement

F. Giannazzo: Conceptualization, Funding acquisition, Project administration, Supervision, Writing – original draft, Writing – review & editing. **S.E. Panasci:** Investigation, Formal analysis, Writing – review & editing. **E. Schilirò:** Investigation, Formal analysis, Writing – review & editing. **G. Greco:** Investigation, Writing – review & editing. **F. Roccaforte:** Project administration, Writing – review & editing. **G. Sfuncia:**

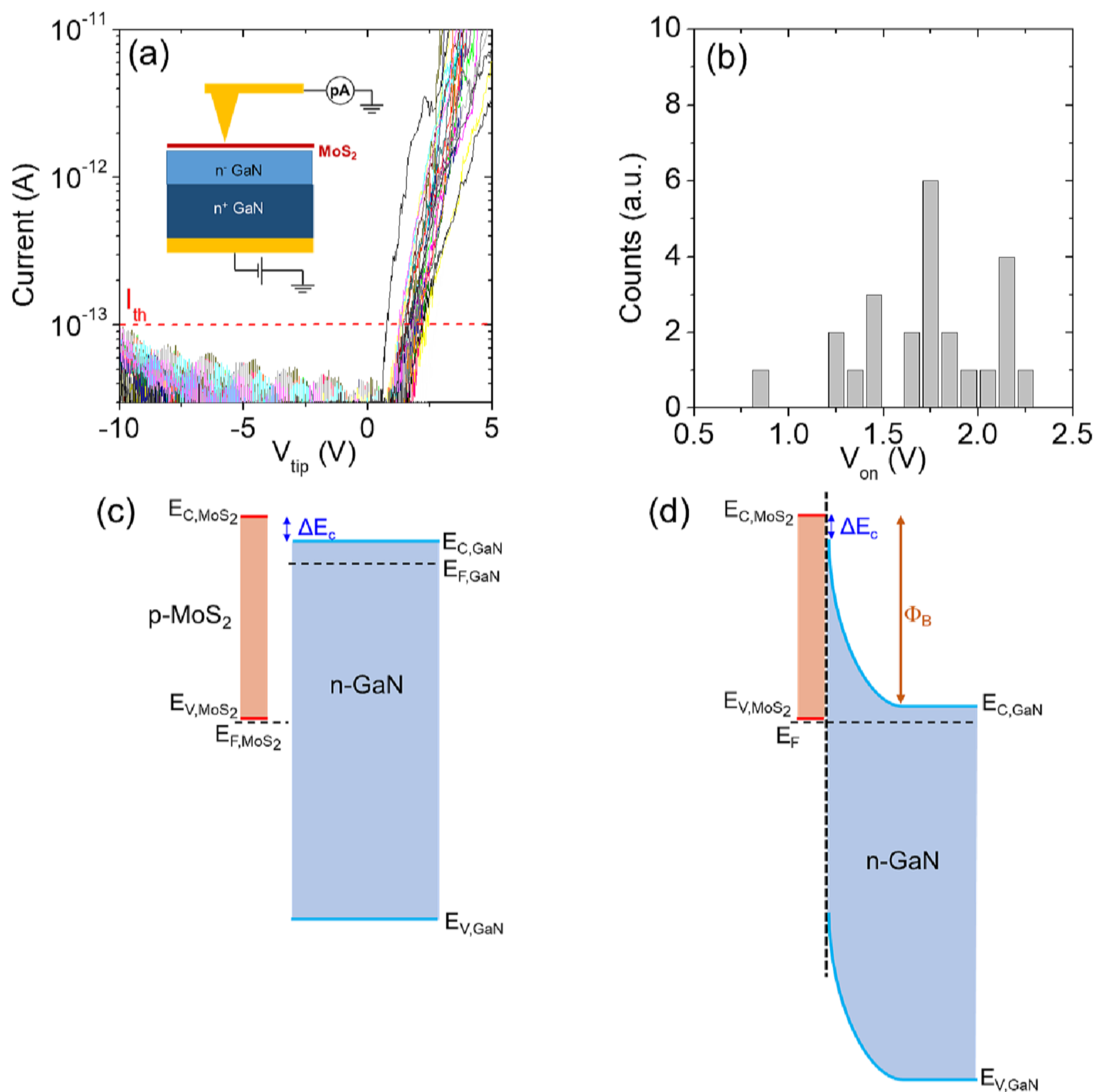

Fig. 6. (a) Set of current-voltage (I-V_{tip}) characteristics collected by C-AFM in the front-to-back configuration (see insert) over an array of 25 tip positions on the MoS_2/GaN heterojunction. (b) Distribution of the onset voltage extracted from the I-V_{tip} curves at a fixed current threshold of 10^{-13} A. Energy band diagrams of the heterojunction before (c) and after (d) contact formation under equilibrium conditions.

Investigation, Formal analysis, Writing – review & editing. **G. Nicotra:** Investigation, Formal analysis, Writing – review & editing. **M. Cannas:** Resources, Writing – review & editing. **S. Agnello:** Resources, Writing – review & editing. **E. Frayssinet:** Resources, Writing – review & editing. **Y. Cordier:** Resources, Writing – review & editing. **A. Michon:** Resources, Writing – review & editing. **A. Koos:** Investigation, Writing – review & editing. **B. Pécz:** Funding acquisition, Investigation, Writing – review & editing.

Declaration of Competing Interest

The authors declare that they have no known competing financial interests or personal relationships that could have appeared to influence the work reported in this paper.

Data availability

Data will be made available on request.

Acknowledgement

S. Di Franco (CNR-IMM, Catania) is acknowledged for the expert technical assistance with sample preparation. We thank N. Nemeth (EK) for XPS measurements, and K. Kandrai, P. Kun, G. Zoltan Radnoczi (EK) for their contribution in MoS_2 films transfer experiments and TEM analyses. P. Fiorenza (CNR-IMM, Catania), F. M. Gelardi (Univ. of Palermo), M. Al Khalfioui (Université Côte d'Azur, CNRS-CRHEA) are acknowledged for useful discussions. This work has been funded, in part, by MUR in the framework of the FlagERA-JTC 2019 project ETMOS. Funding from CNR/HAS bilateral project GHOST-III for traveling is also acknowledged. E.S. acknowledges funding from the ECSEL JU project GaN4AP (Grant Agreement No. 101007310). B.P. and A.K. acknowledge

funding from the national projects TKP2021-NKTA-05 and NKFIH K_134258. The CNR-IMM and Univ. of Palermo acknowledge funding from the "SiciliAn Micro and NanO TecHnology Research and InnovAtion Center (Samothrace)". Part of the experiments was carried out using the facilities of the Italian Infrastructure Beyond Nano.

Appendix A. Supplementary data

Supplementary data to this article can be found online at https://doi.org/10.1016/j.apsusc.2023.157513.

References

[1] Q.H. Wang, K. Kalantar-Zadeh, A. Kis, J.N. Coleman, M.S. Strano, Nat. Nanotechnol. 7 (2012) 699.

[2] E.W. Lee II, L. Ma, D.N. Nath, C.H. Lee, A. Arehart, Y. Wu, S. Rajan, Growth and electrical characterization of two-dimensional layered MoS_2/SiC heterojunctions, Appl. Phys. Lett. 105 (2014), 203504.

[3] Y. Xiao, L. Min, X. Liu, W. Liu, U. Younis, T. Peng, X. Kang, X. Wu, S. Ding, D. W. Zhang, Facile integration of MoS_2/SiC photodetector by direct chemical vapor deposition, Nanophotonics 9 (2020) 3035.

[4] M. Tangi, P. Mishra, T.K. Ng, M.N. Hedhili, B. Janjua, M.S. Alias, D.H. Anjum, C. C. Tseng, Y. Shi, H.J. Joyce, L.L. Li, B.S. Ooi, Determination of band offsets at GaN/single-layer MoS_2 heterojunction, Appl. Phys. Lett. 109 (2016), 032104.

[5] M. Moun, R. Singh, Exploring conduction mechanism and photoresponse in P-GaN/n-MoS_2 heterojunction diode, J. Appl. Phys. 127 (2020), 135702.

[6] S.K. Jain, R.R. Kumar, N. Aggarwal, P. Vashishtha, L. Goswami, S. Kuriakose, A. Pandey, M. Bhaskaran, S. Walia, G. Gupta, Current Transport and Band Alignment Study of MoS_2/GaN and MoS_2/AlGaN Heterointerfaces for Broadband Photodetection Application, ACS Appl. Elect. Mat. 2 (2020) 710.

[7] A. Splendiani, L. Sun, Y. Zhang, T. Li, J. Kim, C.Y. Chim, G. Galli, F. Wang, Emerging Photoluminescence in Monolayer MoS_2, Nano Lett. 4 (2010) 1271.

[8] K.F. Mak, C. Lee, J. Hone, J. Shan, T.F. Heinz, Atomically thin MoS_2: a new direct-gap semiconductor, Phys. Rev. Lett. 105 (2010), 136805.

[9] B. Radisavljevic, A. Radenovic, J. Brivio, V. Giacometti, A. Kis, Single-layer MoS_2 transistors, Nat. Nanotechnol. 6 (2011) 147.

[10] T. Kimoto, J.A. Cooper, Fundamentals of Silicon Carbide Technology: Growth, Characterization, John Wiley & Sons, Devices and Applications, 2014.

[11] F. Roccaforte, P. Fiorenza, G. Greco, R. Lo Nigro, F. Giannazzo, F. Iucolano, M. Saggio, Emerging trends in wide band gap semiconductors (SiC and GaN) technology for power devices, Microelec. Engin. 187 (2018) 66.

[12] E.W. Lee II, C.H. Lee, P.K. Paul, L. Ma, W.D. McCulloch, S. Krishnamoorthy, Y. Wu, A.R. Arehart, S. Rajan, Layer-transferred MoS_2/GaN PN diodes, Appl. Phys. Lett. 107 (2015), 103505.

[13] S. Krishnamoorthy, E.W. Lee II, C.H. Lee, Y. Zhang, W.D. McCulloch, J.M. Johnson, J. Hwang, Y. Wu, S. Rajan, High current density 2D/3D MoS_2/GaN Esaki tunnel diodes, Appl. Phys. Lett. 109 (2016), 183505.

[14] C.Y. Huang, C. Chang, G.Z. Lu, W.C. Huang, C.S. Huang, M.L. Chen, T.N. Lin, J. L. Shen, T.Y. Lin, Hybrid 2D/3D MoS_2/GaN heterostructures for dual functional photoresponse, Appl. Phys. Lett. 112 (2018), 233106.

[15] M. Moun, M. Kumar, M. Garg, R. Pathank, R. Singh, Understanding of MoS_2/GaN Heterojunction Diode and its Photodetection Properties, Sci. Rep. 8 (2018) 1.

[16] D. Ruzmetov, K. Zhang, G. Stan, B. Kalanyan, G.R. Bhimanapati, S.M. Eichfeld, R. A. Burke, P.B. Shah, T.P. O'Regan, F.J. Crowne, A.G. Birdwell, J.A. Robinson, A. V. Davydov, T.G. Ivanov, Vertical 2D/3D Semiconductor Heterostructures Based on Epitaxial Molybdenum Disulfide and Gallium Nitride, ACS Nano 10 (2016) 3580.

[17] T.P. O'Regan, D. Ruzmetov, M.R. Neupane, R.A. Burke, A.A. Herzing, K. Zhang, A. G. Birdwell, D.E. Taylor, E.F.C. Byrd, S.D. Walck, A.V. Davydov, J.A. Robinson, T. G. Ivanov, Structural and electrical analysis of epitaxial 2D/3D vertical heterojunctions of monolayer MoS_2 on GaN, Appl. Phys. Lett. 111 (2017), 051602.

[18] C.R. Serrao, A.M. Diamond, S.-L. Hsu, L. You, S. Gadgil, J. Clarkson, C. Carraro, R. Maboudian, C. Hu, S. Salahuddin, Highly crystalline MoS_2 thin films grown by pulsed laser deposition, Appl. Phys. Lett. 106 (2015), 052101.

[19] Š. Chromik, M. Sojková, V. Vretenár, A. Rosová, E. Dobročka, M. Hulman, Influence of GaN/AlGaN/GaN (0001) and Si (100) substrates on structural properties of extremely thin MoS_2 films grown by pulsed laser deposition, Appl. Surf. Sci. 395 (2017) 232–236.

[20] F. Giannazzo, S.E. Panasci, E. Schilirò, P. Fiorenza, G. Greco, F. Roccaforte, M. Cannas, S. Agnello, A. Koos, B. Pécz, M. Španková, Š. Chromik, Highly Homogeneous 2D/3D Heterojunction Diodes by Pulsed Laser Deposition of MoS_2 on Ion Implantation Doped 4H-SiC, Adv. Mater. Interfaces 10 (2023) 2201502.

[21] F. Giannazzo, S.E. Panasci, E. Schilirò, F. Roccaforte, A. Koos, M. Nemeth, B. Pécz, Esaki Diode Behavior in Highly Uniform MoS_2/Silicon Carbide Heterojunctions, Adv. Mat. Interf. 9 (2022) 2200915.

[22] F. Roccaforte, P. Fiorenza, R. Lo Nigro, F. Giannazzo, G. Greco, Physics and technology of gallium nitride materials for power electronics, Rivista del Nuovo Cimento 41 (2018) 625–681.

[23] S. Chowdhury, D. Ji, Vertical GaN Power Devices, Chapt. 5 of Nitride Semiconductor Technology: Power Electronics and Optoelectronic Devices, eds. F. Roccaforte and M. Leszczynski (Weinheim: Wiley-VCH Verlag) pp. 177–197.

[24] R. Kucharski, T. Sochacki, B. Lucznik, M. Bockowski, Growth of bulk GaN crystals, J. Appl. Phys. 128 (2020), 050902.

[25] P. Desai, A.K. Ranade, M. Shinde, B. Todankar, R.D. Mahyavanshi, M. Tanemura, G. Kalita, Growth of uniform MoS_2 layers on free-standing GaN semiconductor for vertical heterojunction device application, J. Mater. Sci. Mater. Electron. 31 (2020) 2040–2048.

[26] S.E. Panasci, A. Koos, E. Schilirò, S. Di Franco, G. Greco, P. Fiorenza, F. Roccaforte, S. Agnello, M. Cannas, F.M. Gelardi, A. Sulyok, M. Nemeth, B. Pécz, F. Giannazzo, Multiscale Investigation of the Structural, Electrical and Photoluminescence Properties of MoS_2 Obtained by MoO_3 Sulfurization, Nanomaterials 12 (2022) 182.

[27] S. Mignuzzi, A.J. Pollard, N. Bonini, B. Brennan, I.S. Gilmore, M.A. Pimenta, D. Richards, D. Roy, Effect of disorder on Raman scattering of single-layer MoS_2, Phys. Rev. B 91 (2015), 195411.

[28] R.I. Romanov, M.G. Kozodaev, D.I. Myakota, A.G. Chernikova, S.M. Novikov, V. S. Volkov, A.S. Slavich, S.S. Zarubin, P.S. Chizhov, R.R. Khakimov, A.A. Chouprik, C.S. Hwang, A.M. Markeev, Synthesis of Large Area Two-Dimensional MoS_2 Films by Sulfurization of Atomic Layer Deposited MoO_3 Thin Film for Nanoelectronic Applications, ACS Appl. Nano Mater. 2 (2019) 7521.

[29] S. Baek, J. Kim, S. Choo, A. Sen, B. Jang, P. Pujar, S. Kim, H.-J. Kwon, Low-Temperature Carrier Transport Mechanism of Wafer-Scale Grown Polycrystalline Molybdenum Disulfide Thin-Film Transistor Based on Radio Frequency Sputtering and Sulfurization, Adv. Mater. Interfaces 9 (2022) 2102360.

[30] Y.-C. Lin, W. Zhang, J.-K. Huang, K.-K. Liu, Y.-H. Lee, C.-T. Liang, C.-W. Chu, L.-J. Li, Wafer-scale MoS_2 thin layers prepared by MoO_3 sulfurization, Nanoscale 4 (2012) 6637.

[31] M.H. Heyne, D. Chiappe, J. Meersschaut, T. Nuytten, T. Conard, H. Bender, C. Huyghebaert, I.P. Radu, M. Caymax, J.-F. de Marneffe, E.C. Neyts, S. De Gendt, Multilayer MoS_2 growth by metal and metal oxide sulfurization, J. Mater. Chem. C 4 (2016) 1295.

[32] I.V. Zabrosaev, M.G. Kozodaev, R.I. Romanov, A.G. Chernikova, P. Mishra, N. V. Doroshina, A.V. Arsenin, V.S. Volkov, A.A. Koroleva, A.M. Markeev, Field-Effect Transistor Based on 2D Microcrystalline MoS_2 Film Grown by Sulfurization of Atomically Layer Deposited MoO_3, Nanomaterials 12 (2022) 3262.

[33] H. Li, Q. Zhang, C.C.R. Yap, B.K. Tay, T.H.T. Edwin, A. Olivier, D. Baillargeat, From Bulk to Monolayer MoS_2: Evolution of Raman Scattering, Adv. Funct. Mat. 22 (2012) 1385.

[34] X. Zhang, X.F. Qiao, W. Shi, J.B. Wu, D.S. Jiang, P.H. Tan, Phonon and Raman scattering of two-dimensional transition metal dichalcogenides from monolayer, multilayer to bulk material, Chem. Soc. Rev. 44 (2015) 2757.

[35] S.E. Panasci, E. Schilirò, G. Greco, M. Cannas, F.M. Gelardi, S. Agnello, F. Roccaforte, F. Giannazzo, Strain, Doping, and Electronic Transport of Large Area Monolayer MoS_2 Exfoliated on Gold and Transferred to an Insulating Substrate, ACS Appl. Mat. Interf. 13 (2021) 31248.

[36] A. Michail, N. Delikoukos, J. Parthenios, C. Galiotis, K. Papagelis, Optical detection of strain and doping inhomogeneities in single layer MoS_2, Appl. Phys. Lett. 108 (2016), 173102.

[37] D. Lloyd, X. Liu, N. Boddeti, L. Cantley, R. Long, M.L. Dunn, J. Scott Bunch, Adhesion, Stiffness, and Instability in Atomically Thin MoS_2 Bubbles, Nano Lett. 17 (2017) 5329–5334.

[38] B. Chakraborty, A. Bera, D.V.S. Muthu, S. Bhowmick, U.V. Waghmare, A.K. Sood, Symmetry-dependent phonon renormalization in monolayer MoS_2 Transistor, Phys. Rev. B 85 (2012), 161403.

[39] Z. Zhang, Q. Qian, B. Li, K.J. Chen, Interface Engineering of Monolayer MoS_2/GaN Hybrid Heterostructure: Modified Band Alignment for Photocatalytic Water Splitting Application by Nitridation Treatment, ACS Appl. Mat. Interf. 10 (2018) 17419.

[40] V. Bougrov, M.E. Levinshtein, S.L. Rumyantsev, A. Zubrilov, in: Properties of Advanced Semiconductor Materials GaN, AlN, InN, BN, SiC, SiGe . Eds. Levinshtein, M.E.; Rumyantsev, S.L.; Shur M.S., John Wiley & Sons, Inc., New York, 2001, pp. 1-30.